atmosphere

MDPI

Article

Long-Term COVID-19 Restrictions in Italy to Assess the Role of Seasonal Meteorological Conditions and Pollutant Emissions on Urban Air Quality

Giovanni Gualtieri *, Lorenzo Brilli, Federico Carotenuto, Carolina Vagnoli, Alessandro Zaldei and Beniamino Gioli

National Research Council, Institute of Bioecomony (CNR-IBE), Via Caproni 8, 50145 Firenze, Italy; lorenzo.brilli@ibe.cnr.it (L.B.); federico.carotenuto@ibe.cnr.it (F.C.); carolina.vagnoli@ibe.cnr.it (C.V.); alessandro.zaldei@ibe.cnr.it (A.Z.); beniamino.gioli@cnr.it (B.G.)

* Correspondence: giovanni.gualtieri@ibe.cnr.it; Tel.: +39-55-303-3743

Abstract: A year-round air quality analysis was addressed over four Italian cities (Milan, Turin, Bologna, and Florence) following the outbreak of the Coronavirus 2019 (COVID-19) pandemic. NO_2, O_3, $PM_{2.5}$, and PM_{10} daily observations were compared with estimations of meteorological variables and observations of anthropogenic emission drivers as road traffic and heating systems. Three periods in 2020 were analysed: (i) the first (winter/spring) lockdown, (ii) the (spring/summer) partial relaxation period, and (iii) the second (autumn/winter) lockdown. During the first lockdown, only NO_2 concentrations decreased systematically (and significantly, between −41.9 and −53.9%), mainly due to the drastic traffic reduction (−70 to −74%); $PM_{2.5}$ varied between −21 and +18%, PM_{10} varied between −23 and +9%, and O_3 increased (up to +17%). During the partly relaxation period, no air quality issues were observed. The second lockdown was particularly critical as, although road traffic significantly reduced (−30 to −44%), $PM_{2.5}$ and PM_{10} concentrations dramatically increased (up to +87 and +123%, respectively), mostly due to remarkably unfavourable weather conditions. The latter was confirmed as the main driver of PM's most critical concentrations, while strong limitations to anthropogenic activity—including traffic bans—have little effect when taken alone, even when applied for more than two months and involving a whole country.

Keywords: COVID-19; air quality; PM_{10}; lockdown; road traffic; Italy

Citation: Gualtieri, G.; Brilli, L.; Carotenuto, F.; Vagnoli, C.; Zaldei, A.; Gioli, B. Long-Term COVID-19 Restrictions in Italy to Assess the Role of Seasonal Meteorological Conditions and Pollutant Emissions on Urban Air Quality. *Atmosphere* **2022**, *13*, 1156. https://doi.org/10.3390/atmos13071156

Academic Editors: Ruixiong Zhang, Tzung May Fu, Deborah S. Gross and Andrey Khlystov

Received: 21 June 2022
Accepted: 20 July 2022
Published: 21 July 2022

1. Introduction

Since the early days of the COVID-19 pandemic outbreak, the scientific community has been constantly engaged in investigating the underlying patterns of the pandemic. The mechanisms triggering its spread worldwide, its environmental and socio-economic impacts, and the most effective countermeasures to be taken have been extensively addressed [1]. These countermeasures led to rapid and unprecedented decreases in social and economic activities that resulted—among others—in modifications in the emissions of air pollutants and greenhouse gases. This worldwide event thus turned into a kind of "extreme" real-world experiment that offered a unique scientific opportunity to investigate the impacts of modified anthropogenic emissions on atmospheric composition at regional to global spatial scales [2]. As a result, a huge body of research has been published on various environmental issues related to the COVID-19 pandemic, as documented by several review articles (e.g., [1–5]).

In addition to the vast majority of studies focusing on the lockdown period, a remarkable body of literature has also been established analysing the post-lockdown scenario, marked by a partial or full relaxation of the restriction measures (e.g., [6–9]). However, a research gap found in these studies is a comprehensive investigation of air quality

pattern during the entirety of 2020. The first lockdown and the subsequent partial/total relaxation period (typically lasting up to August/September 2020) were generally addressed, whereas the severe lockdown measures enforced during the last months of 2020 to tackle the effects of the second and third wave of the pandemic were rarely studied (e.g., [10]). Furthermore, late 2020 lockdown measures were taken in a period that in Italy is more meaningful in terms of air quality than the first lockdown, as it is characterized by emission pressures and weather conditions that are more harmful to the population. Of note, the lack of late 2020 analysis was highlighted by [9] as a clear limitation to their comprehensive study addressed over 25 countries and 63 cities worldwide. A year-round approach offers the advantage of characterizing the seasonal dynamics, taking into account all possible combinations of both meteorological and emission conditions, as well as separating their relative role in controlling pollutant mixing ratios.

The main contribution of the present study is thus aimed at filling/integrating this research gap by targeting the following goals: (i) to assess how urban air quality changed in Italy over the year 2020 during all restriction periods enforced after the COVID-19 outbreak compared to a "baseline" scenario, (ii) to specifically focus on the effects of 2020 autumn/winter lockdown scenario on air quality, and (iii) to investigate the role played by main meteorological drivers and pollutant emissions on atmospheric pollution in urban areas.

Most of the research studies analysing the impact of 2020 lockdown measures on air quality were addressed based on direct comparison against a "baseline" period, when "business as usual" emissions prevailed. Consistent with several authors (e.g., [6,11–16]), the year immediately preceding the pandemic (2019) was used as a baseline in this study. The stringency index (SI [17]), a unified, globally consistent indicator for the severity of lockdown measures taken by governments frequently used in similar studies (e.g., [2,18,19]), was adopted to discriminate three distinct restriction periods: (i) the first (winter/spring) lockdown (labelled as Lock_1), (ii) the (spring/summer) period of partially relaxed restrictions (Soft), and (iii) the second (autumn/winter) lockdown (Lock_2). Accordingly, three seasonally mirrored periods in 2019 were selected as a baseline for direct comparison. The analysis focused on four major cities in central and northern Italy: Turin, Milan, Bologna, and Florence. Daily observations of air pollutant concentrations such as nitrogen dioxide (NO_2), ozone (O_3), and particulate matter with an aerodynamic diameter lower than 2.5 μm ($PM_{2.5}$) and 10 μm (PM_{10}) were collected from ground-based air quality stations. Meteorological data were derived as daily estimations by the European Centre for Medium-Range Weather Forecasts (ECMWF) Reanalysis 5th Generation (ERA5) [20]. Road traffic and heating systems were identified as the main anthropogenic drivers of pollutant emissions over the urban study areas, so measured vehicle counts and estimated gas consumptions were used, respectively.

2. Materials and Methods

2.1. Study Areas

The analysis focused on four urban areas in Italy: Turin, Milan, Bologna, and Florence. Their maps are shown in Figure 1, while their general characteristics are reported in Table S1 of the Supplementary Materials. Turin, Milan, and Bologna lie within the Po Valley in Northern Italy, while Florence is located in the central part of the country.

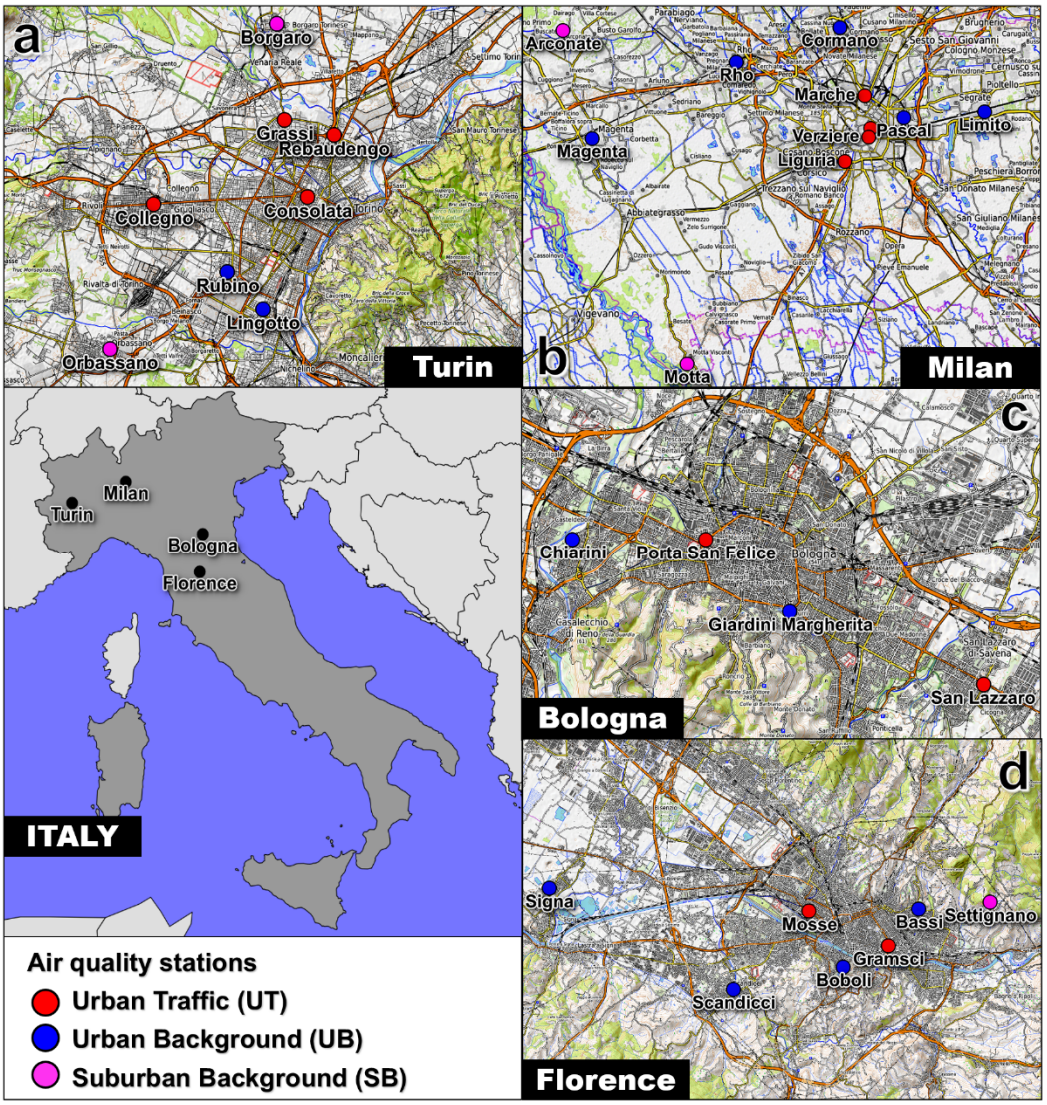

Figure 1. Map of the urban study areas in Italy, also showing location of urban traffic (UT), urban background (UB), and suburban background (SB) air quality stations: (**a**) Turin; (**b**) Milan; (**c**) Bologna; (**d**) Florence. Cartography basemap: OpenTopoMap.

2.2. COVID-19-Induced Restriction Measures

The stringency index (SI) [17] has been identified as an objective metric to provide the chronological dates and strengths of all restriction measures taken following the onset of the COVID-19 pandemic. Introduced to compare the government measures at different times and stages of the pandemic from different regions worldwide, this index returns—on a daily basis and for each country—a value ranging from 0 (no restrictions) to 100 (maximum restrictions). The SI incorporates the nomenclature adopted for classification such as "Full lockdown" or "Full relaxation" [21], "Phase 1" or "Phase 2" [22], and "Normality 1" or "New normality" [6] into a single metric, thus allowing a direct comparison of the strength of different restrictions from one country to another. The full SI dataset [23] may be found at the Oxford COVID-19 government response tracker [24].

In the present analysis, the SI for Italy across the year 2020 was collected (Figure S1). As most countries [19], Italy introduced lockdowns somewhere between the last week of January and the first week of February 2020. The analysis of the SI pattern in Italy (Figure S1) led to the detection of three distinct periods:

- "Lock_1" (winter/spring first lockdown), 24/02/2020–03/05/2020;
- "Soft" (spring/summer partly relaxed restrictions), 04/05/2020–22/10/2020;

- "Lock_2" (autumn/winter second lockdown), 23/10/2020−29/12/2020.

Lock_1 is the period of the first and most stringent restrictions, characterised by SI values ranging from 69.91 to 93.52 (averaging 86.65, Figure S1). It includes the first restrictions limited to the Lombardy and Veneto northern regions, as well as the first lockdown applying to the whole country [16]. Soft, characterised by SI values between 47.22 and 72.22 (averaging 55.84), marks the period of partial relaxation after the first nationwide lockdown. Lock_2, affected by quite constant SI values (74.07–84.26, averaging 78.89), is the period when the second nationwide lockdown was adopted.

Mirroring these 2020 periods, three seasonally similar periods in 2019 were selected as a baseline for comparison (see Section 2.4.). The details of both 2020 periods and 2019 baseline periods are reported in Table S2.

2.3. Data

Three data categories have been processed: air quality observations, meteorology estimations, and anthropogenic emissions derived from measured proxy variables. Overall yearly estimates of pollutant emissions from regional inventories have been also analysed to support the analysis. These inventorial data indicated that road traffic and heating systems are the main drivers of anthropogenic emissions over the study areas (see Section 2.3.5.), so proxy variables for these two emitting categories have been selected.

2.3.1. Air Quality

Pollutant concentrations were obtained by the air-quality-monitoring network managed by the regional environmental protection agencies (ARPAs). NO_2, $PM_{2.5}$, and PM_{10} concentrations were derived from urban traffic (UT) and urban background (UB) air quality stations, while O_3 concentrations were derived from suburban background (SB) and UB stations. The location of all (30) air quality stations is shown in Figure 1, while Table S3 reports the details of each station and the measured parameters. Since $PM_{2.5}$ and PM_{10} concentrations were only available on a daily basis, concentrations of the other pollutants have been averaged from hourly to daily values.

2.3.2. Meteorology

Consistent with similar studies (e.g., [9,10]), meteorological data were derived as daily estimations provided by the ERA5 reanalyses [20], which can be downloaded from the online website [25]. ERA5 is the fifth generation and the most updated (2019) global reanalysis product developed by the ECMWF. ERA5 provides 1 h estimates of several atmospheric variables on a regular lat/lon grid of 0.25 by 0.25 deg with global coverage [20], assimilating satellite data as well as in situ observations such as Synop, Metar, radiosounding, wind profiler, radar, aircraft, buoy, and ship data [25]. For the centroid of each urban area, ERA5 daily data of the following parameters were extracted: wind speed (*WS*), air temperature (*T*), planetary boundary layer (PBL) height (*H*), downward shortwave radiation (*R_dsw*), and precipitation (*Prec*).

2.3.3. Gas Consumption

Based on statistics by [26], natural gas (methane) is the predominant fuel used for heating plants in Italy (with average shares of 78% in Florence, and of 89.1% over the climatic zone comprising Turin, Milan, and Bologna), so its consumption can account for the usage of heating plants. Accordingly, data on natural gas (simply "gas" hereafter) consumption were assumed as a reasonable proxy of pollutant emissions from other fuel combustion heating plants, such as biomass and oil burning [27]. Data on gas consumption have been provided by Estra SpA (https://www.estra.it (accessed on 21 July 2022)) only for the city of Florence for the first six months of years 2019 and 2020. To cope with the lack of data for the other cities, based on Florence data, a regression analysis was carried out to express the daily normalized gas consumption as a function of daily mean

temperature. This was performed by categorizing the whole dataset by 0.5 °C temperature intervals and then calculating the mean values of both temperature and gas consumption over each interval. The linear best-fit of the regression analysis applied to this dataset exhibited a clear inflection point, which was found at T = 15 °C. Data were then split into two subsets discriminated by this T value, so the following two best-fit equations (affected by R^2 values of 0.984 and 0.305, respectively) were achieved:

$$Gas = -0.161*T + 2.694, \text{ for } T \leq 15\ ^\circ\text{C} \quad (1)$$

$$Gas = -0.005*T + 0.385, \text{ for } T > 15\ ^\circ\text{C} \quad (2)$$

where *Gas* (dimensionless) is the daily gas consumption normalised to the whole municipality and to the 2019–2020 average, and T (°C) is the municipality-averaged daily air temperature (Figure S2).

Equations (1) and (2) can be applied to any city, comparable in terms of climate zoning and heating usage. In the present analysis, they were also used as a proxy of gas consumption data over the second six months of the year.

The daily pattern of gas consumption calculated for all study areas in 2020 is plotted in Figure S3a.

2.3.4. Road Traffic

Air pollutant emissions from road vehicles have been assessed by collecting road mobility information over each study area. Road traffic data have been retrieved from daily averaged vehicle counts measured by each municipality. For the city of Turin, mobility data have been directly received by the "5T srl" company [28]. For the cities of Milan and Bologna, traffic data have been downloaded by their respective open data repositories, managed by the Municipality of Milan [29] and the Municipality of Bologna [30], respectively. For the city of Florence, mobility data have been downloaded by the Snap4City platform [31].

The daily pattern of road traffic flows observed over all urban areas in 2020 is plotted in Figure S3b in terms of relative variation to the year 2019. Unfortunately, traffic flow data sorted by vehicle type were not available for any city.

2.3.5. Inventorial Pollutant Emissions

To assess the role played by different emitting categories, data from the most updated versions of the following regional emission inventories have been analysed: Turin (updated to 2015 [32]); Milan (2017 [33]); Bologna (2017 [34]); Florence (2017 [35]). Since these data are annual overall estimates—and not concurrent with the period under examination—they were not processed in the inference analysis but were used solely to support the discussion of the results. For each study area, the share by EU SNAP category of the overall municipality-scale yearly emissions of NO_x, NH_3, and primary $PM_{2.5}$ and PM_{10} has been summarized in Table S4. The combined weight of energy and transformation industries (SNAP category 01) and the manufacturing industry (03) on pollutant emissions is minor. For NO_x, for example, these two categories contribute to overall emissions by 28.1% in Turin, 10.7% in Milan, 8.2% in Florence, and 5.3% in Bologna; for primary PM_{10}, they contribute by 8% in Milan, 2.3% in Turin, 0.7% in Bologna, and 0.7% in Florence. The contribution of these two sectors was therefore ruled out from the analysis. As for NH_3 emissions from the agriculture sector (10), over 68% of the nationwide contribution comes from the Po Valley in Northern Italy: based on 2019 data, 25.5% is emitted in the Lombardy region, 10.3% in Piedmont, and 12.3% in Emilia-Romagna, while the contribution from Tuscany is remarkably lower (1.8% [36]). At the municipality level, after processing the values reported in Table S4, the contribution of agriculture to NH_3 emissions is 66.1 t/y in Milan, 41.7 t/y in Bologna, 21.4 t/y in Florence, and 13.9 t/y in Turin. However, NH_3 emission data from agriculture (or proxies suitably reproducing their pattern) were not available, either at a municipality or country level. Therefore, road traffic and heating

plants ultimately proved to be the main drivers of anthropogenic emissions over the study areas and were therefore selected for the inference analysis. Because of the specific focus on gas consumption and road traffic, in Table S5, the shares by fuel type of yearly emissions from non-industrial combustion plants (SNAP category 02) are provided, while in Table S6, the shares by vehicle category of total emissions from road transport (07) are provided.

2.4. Methods

In order to quantify the effects caused by the COVID-19 restrictions on air quality in urban areas in the year 2020, for each of the three 2020 restriction periods defined in Section 2.2., a "business as usual" scenario was set as a reference by selecting the seasonally mirrored periods in the year 2019 (Table S2).

Overall, for each year, datasets included 310 daily time series of the following 15 variables: (i) for meteorology, *WS*, *T*, *H*, *R_dsw*, and *Prec*; (ii) for drivers of anthropogenic emissions, municipality-averaged gas consumption and road traffic flows; (iii) for air quality, concentrations of O_3 at SB and UB stations as well as concentrations of NO_2, $PM_{2.5}$, and PM_{10} at UT and UB stations. When multiple air quality stations of a given type were available in the monitoring network of an urban area, concentration data were averaged across all stations of the same type (Table S3).

All computations were performed using the "R-stat" environment v. 4.0.3 [37], while the frequency distribution was analysed in terms of boxplots using the "boxplot" function implemented in the R Graphics Package [38].

A further analysis was made on the Lock_2 period using Self-Organizing Maps (SOMs), an unsupervised learning ANN-based model that implements a nonlinear projection from a high-dimensional space of input signals to a regular (usually 2-D) grid of neurons [39]. Thus, complex, nonlinear statistical relationships between high-dimensional data are converted into simple geometric relationships on a low-dimensional display. The SOMs recognize clusters of similar input variables and map the neurons with similar feature values close to each other, while neurons with dissimilar values are mapped on different edges. This makes visualization of the grid useful in investigating the relationship between variables and the possible cluster structure of the data [39]. SOMs were calculated using the "Living for SOM" tool (http://livingforsom.com (accessed on 21 July 2022)).

3. Results

Figures S4–S7 show the boxplots of NO_2, O_3, $PM_{2.5}$, and PM_{10} daily concentrations measured by station type over all urban areas during each 2020 period as compared to its corresponding baseline period in 2019. To assess the differences among periods affecting the analysed variables and the possible relations with meteorology and anthropogenic drivers, in Figures 2–5, the boxplots of 2020 vs. 2019 change rates are plotted for the same pollutant concentrations as well as for main meteorological parameters (*WS*, *T* and *H*), gas consumption and road traffic. In Table S7, the median values by period of all variables processed across the years 2019 and 2020 are summarised along with their corresponding median change rates.

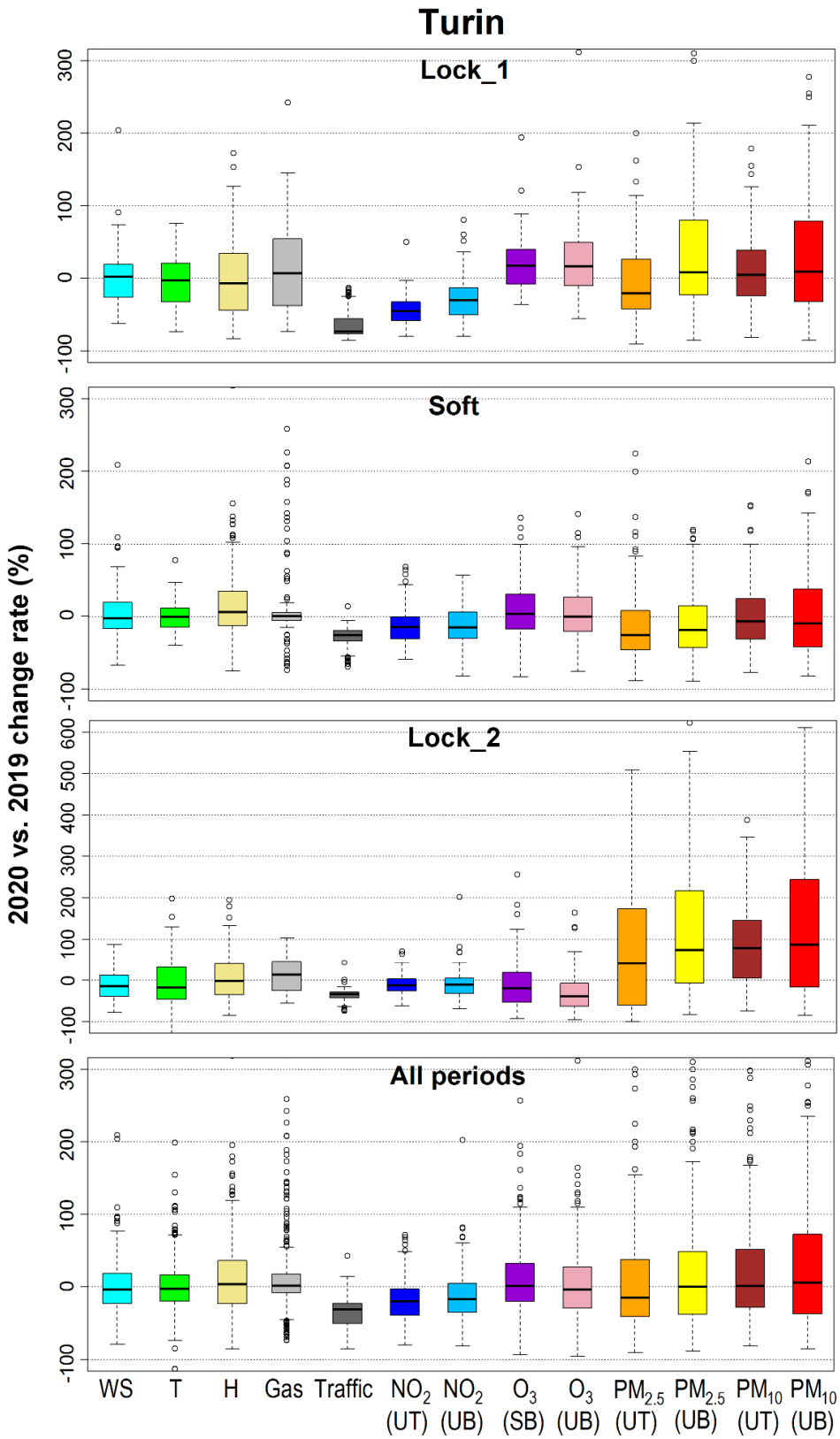

Figure 2. Boxplots by period of 2020 vs. 2019 change rates of daily observations in Turin: concentrations by station type of NO_2, O_3, $PM_{2.5}$, and PM_{10}; wind speed (*WS*); air temperature (*T*); PBL height (*H*), gas consumption; road traffic. Boxplots are delimited by the first (Q_1) and third (Q_3) distribution's quartiles, while the black line inside the box denotes the median value (Q_2). Lower whisker is $Q_1 - 1.5*IQR$, while upper whisker is $Q_3 + 1.5*IQR$, where the interquartile range (*IQR*) is $Q_3 - Q_1$. Circles outside the whiskers denote outlier data.

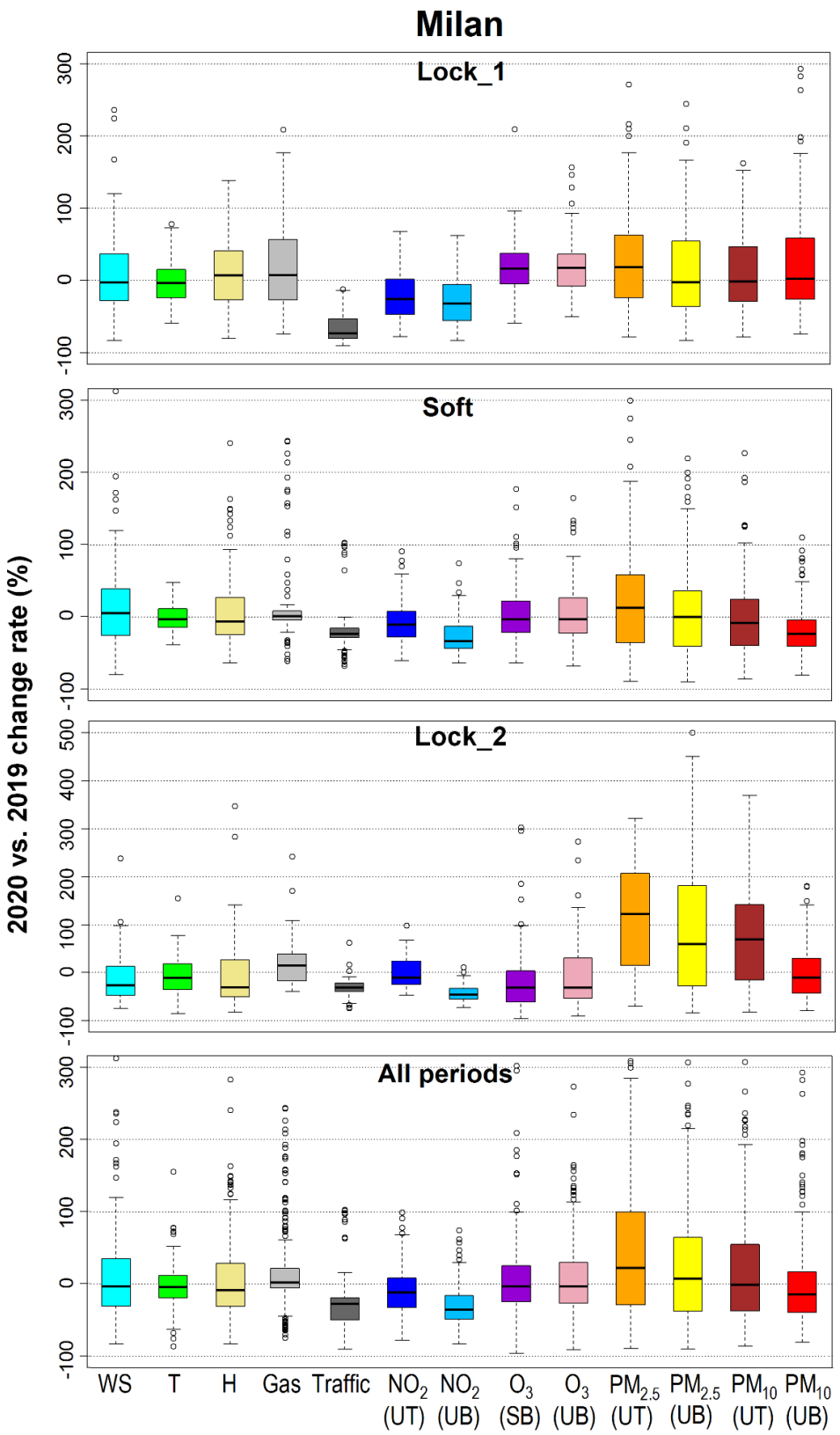

Figure 3. Boxplots by period of 2020 vs. 2019 change rates of daily observations in Milan: concentrations by station type of NO_2, O_3, $PM_{2.5}$, and PM_{10}; wind speed (*WS*); air temperature (*T*); PBL height (*H*), gas consumption; road traffic. Boxplots are delimited by the first (Q_1) and third (Q_3) distribution's quartiles, while the black line inside the box denotes the median value (Q_2). Lower whisker is $Q_1 - 1.5*IQR$, while upper whisker is $Q_3 + 1.5*IQR$, where the interquartile range (*IQR*) is $Q_3 - Q_1$. Circles outside the whiskers denote outlier data.

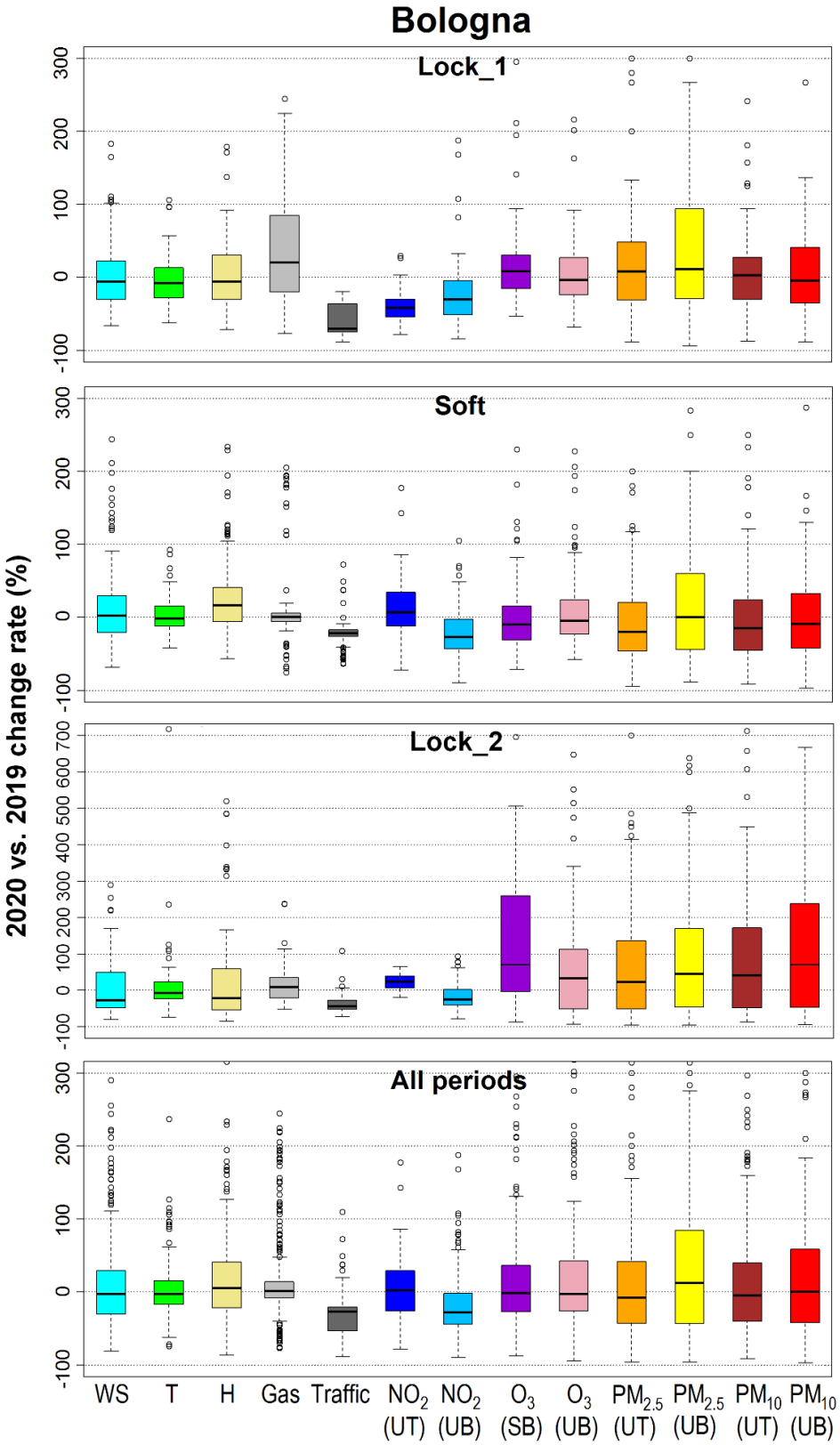

Figure 4. Boxplots by period of 2020 vs. 2019 change rates of daily observations in Bologna: concentrations by station type of NO_2, O_3, $PM_{2.5}$, and PM_{10}; wind speed (*WS*); air temperature (*T*); PBL height (*H*), gas consumption; road traffic. Boxplots are delimited by the first (Q_1) and third (Q_3) distribution's quartiles, while the black line inside the box denotes the median value (Q_2). Lower whisker is $Q_1 - 1.5*IQR$, while upper whisker is $Q_3 + 1.5*IQR$, where the interquartile range (*IQR*) is $Q_3 - Q_1$. Circles outside the whiskers denote outlier data.

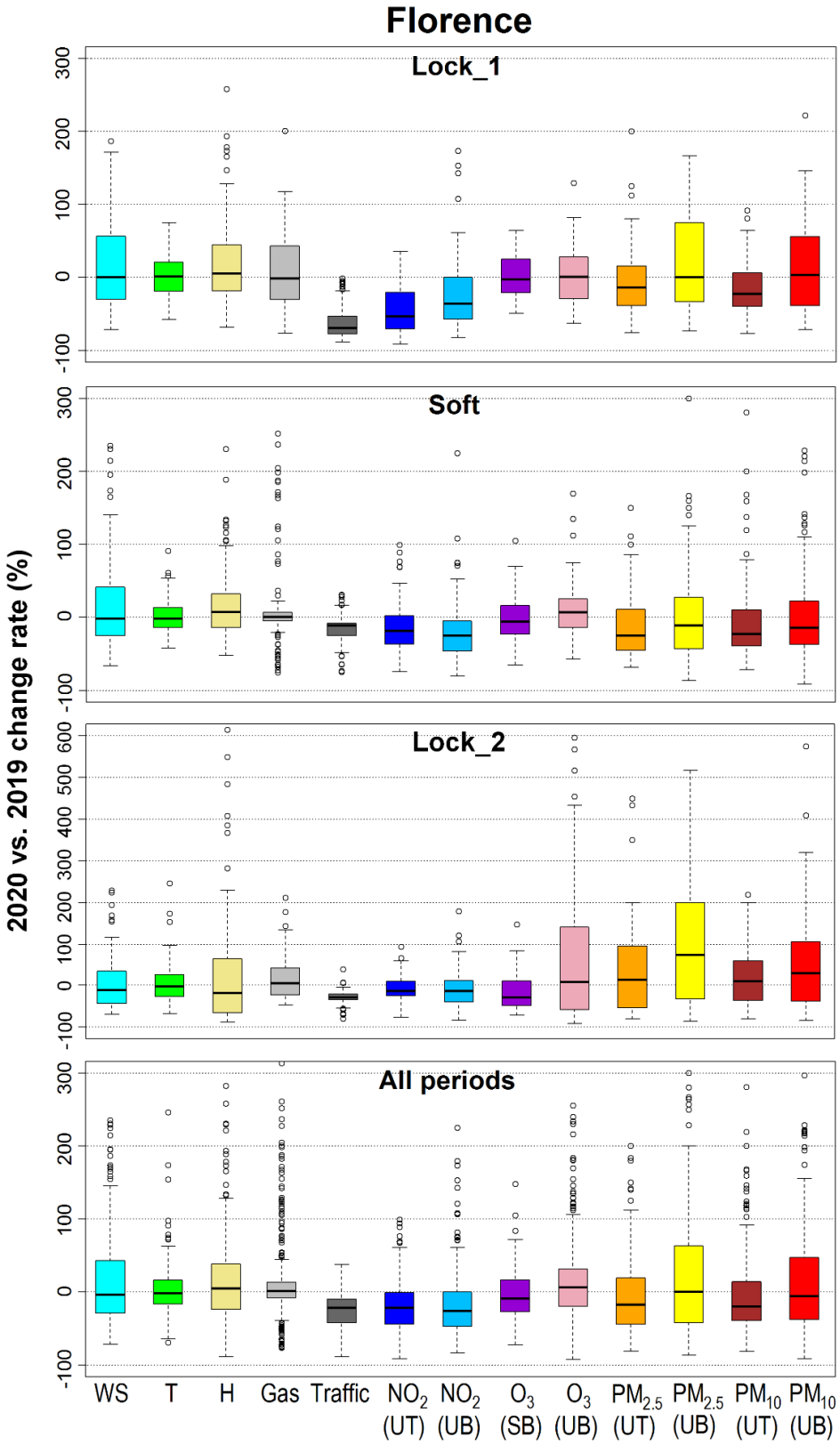

Figure 5. Boxplots by period of 2020 vs. 2019 change rates of daily observations in Florence: concentrations by station type of NO_2, O_3, $PM_{2.5}$, and PM_{10}; wind speed (*WS*); air temperature (*T*); PBL height (*H*), gas consumption; road traffic. Boxplots are delimited by the first (Q_1) and third (Q_3) distribution's quartiles, while the black line inside the box denotes the median value (Q_2). Lower whisker is $Q_1 - 1.5*IQR$, while upper whisker is $Q_3 + 1.5*IQR$, where the interquartile range (*IQR*) is $Q_3 - Q_1$. Circles outside the whiskers denote outlier data.

3.1. Turin

In Turin, 2020 road mobility exhibited a clear reduction with respect to 2019, with median values of −74% during Lock_1, −25% during Soft, and −34% during Lock_2 (Table S7). By contrast, gas consumption slightly increased across all restriction periods, by +7, +1 and +9%, respectively, likely because of the generalized decrease in *T* (from −0.2 to −1 °C). As also shown by the boxplots of 2020 vs. 2019 change rate (Figure 2), 2020 meteorological conditions were basically the same as in the previous year during Soft, while reductions in *WS*, *H* and *Prec* were recorded during Lock_1 and particularly Lock_2. A clear reduction in NO_2 concentrations was observed, higher during Lock_1 (−31 to −45.4%, up to -24.3 μg/m^3) than during the other periods (−12 to −15%, up to −9.3 μg/m^3), particularly at UT stations. O_3 concentrations exhibited contrasting behaviour across the three periods (Figure 2), as slightly increasing during Lock_1 (+16 to +17%), remaining basically unchanged during Soft, and significantly decreasing during Lock_2 (−20 to −40%), however low absolute concentrations were measured (at most 10.4 μg/m^3, Figure S4b). The analysis of Figure 2 reveals that $PM_{2.5}$ concentrations decreased during Lock_1 (except at UB stations) and Soft, while they dramatically increased during Lock_2, with median values of +68% (UT) and +75% (UB, Table S7), corresponding to +13.8 and +14 μg/m^3, respectively (Figure S4c). PM_{10} concentrations (Figure S4d) exhibit a similar pattern to $PM_{2.5}$, remaining unchanged or slightly decreasing across the first two periods, while dramatically increasing during Lock_2 (Figure 2), by +79% at UT and +87% at UB stations (Table S7), corresponding to +17.5 and +21.8 μg/m^3, respectively. These PM_{10} increases during Lock_2 resulted in remarkable median concentrations of 45 μg/m^3 at UB and 54.8 μg/m^3 at UT stations (Figure S4d).

3.2. Milan

In Milan, the 2020 vs. 2019 scenario of both selected drivers of anthropogenic emissions (Figure 3) was quite similar to Turin: road traffic decreased by roughly the same amounts (−73% during Lock_1, −24% during Soft, and −32% during Lock_2), while gas consumption increased by +7, +1 and +14%, respectively (Table S7). During the first two periods, 2020 meteorological conditions were basically the same as in the previous year, while a significant change was (again) experienced during Lock_2 (Figure 3), with median reductions of −28% (*WS*), −12% (*T*), −31% (*H*), and −95% (*Prec*, Table S7). Unlike in Turin, the drop observed in NO_2 concentrations during the 2020 periods was higher at UB than at UT stations: at the former, the highest average reductions (−46.5%, i.e., −20.4 μg/m^3) were measured during Lock_2, while at the latter, they were measured during Lock_1 (−26%, i.e., −10.5 μg/m^3). Notably, during the Soft and Lock_2 periods, NO_2 concentrations at UB stations exhibited a very narrow distribution almost entirely peaked around the median value (Figure S5a). In Milan, O_3 concentrations exhibited the same pattern across the three periods (Figure 3) as in Turin, thus slightly increasing during Lock_1 (+16 to +17%), remaining unchanged during Soft, and significantly decreasing during Lock_2 (−32%, Table S7). At UB stations, $PM_{2.5}$ concentrations remained basically unchanged during Lock_1 and Soft, and they were significantly increased during Lock_2 (+60%, Table S7 and Figure 3); at UT stations, $PM_{2.5}$ concentrations slightly increased during the first two periods (+12 to +18%), and they dramatically increased during the third (+123%, Table S7 and Figure 3). Overall, these $PM_{2.5}$ increases spanned between +12.5 and +22 μg/m^3, to reach the remarkable median concentrations of 34 and 42 μg/m^3, respectively (Figure S5c). As for PM_{10} concentrations (Figure 3), at both UT and UB stations, they remained unchanged during Lock_1 and slightly decreased during Soft, while they exhibited a contrasting pattern during Lock_2, increasing (+70%, +16.3 μg/m^3) at UT stations while decreasing (−11%, −4.3 μg/m^3) at UB stations. During Lock_2 UT, the median PM_{10} concentrations were equal to 46.4 μg/m^3 (Figure S5d).

3.3. Bologna

Similar to Turin and Milan, in Bologna, 2020 road traffic median values were reduced by −70% during Lock_1, −22% during Soft, and −44% during Lock_2 (Table S7), while gas consumption increased by +20, +1 and +2%, respectively (Figure 4). The 2020 meteorological scenario exhibited different behaviour across the three periods with respect to the 2019 scenario, particularly as *WS*, *T* and *H* slightly decreased during Lock_1 and Lock_2 while they did not appreciably change during Soft (Figure 4). As also observed in Turin and Milan, *Prec* significantly decreased across all periods (Table S7). In Bologna, at UB stations, NO_2 concentrations returned a steady reduction across the three periods (between −26 and −31%); unlike in all other cities, here, NO_2 concentrations at UT stations appreciably decreased during Lock_1 (up to −16.3 μg/m^3), while they increased during Soft and particularly Lock_2 (Figure 4). O_3 concentrations remained unchanged during the first two periods and increased during the third (up to +4 μg/m^3, Figure S6b). In Bologna, 2020 $PM_{2.5}$ concentrations remained substantially unchanged during Lock_1, slightly decreased during Soft, and increased during Lock_2 (Figure 4), when median increases of +21% (UT) and +44% (UB) were recorded (Table S7). These $PM_{2.5}$ increases during Lock_2 thus varied between +5.5 and +6.5 μg/m^3, resulting in $PM_{2.5}$ median concentrations of 21.5 μg/m^3 (Figure S6c). The pattern of PM_{10} concentrations across the three periods was quite similar to $PM_{2.5}$, yet returning higher increases during Lock_2, by +40% at UT and +70% at UB stations. The latter correspond to increases of +10.3 and +14.5 μg/m^3, respectively, resulting in PM_{10} median concentrations equal to 33.5 μg/m^3 (Figure S6d).

3.4. Florence

Florence's road traffic in 2020 was reduced by a slightly lower amount than elsewhere (Figure 5), i.e., by −70% during Lock_1, −11% during Soft, and –30% during Lock_2 (Table S7). Gas consumption did not change appreciably during the first two periods, while slightly increased (+4%) during Lock_2. The 2020 meteorological conditions were the same as in 2019 except during Lock_2, when slight reductions were observed in *WS* (−12%), *T* (−4%), *H* (−19%) and *Prec* (−79%). A reduction in NO_2 concentrations was observed in 2020, particularly during Lock_1 (up to –53.9%, i.e., −24.7 μg/m^3), and by a lower amount during Soft (−18 to −25%) and Lock_2 (−15%). The O_3 concentrations did not appreciably change during the first two periods, while they significantly decreased during Lock_2 at SB stations (−30%, i.e., −10.7 μg/m^3). The $PM_{2.5}$ concentrations decreased during Lock_1 and Soft (up to −25%, i.e., −3 μg/m^3), while they increased during Lock_2 (up to +75%, i.e., +4 μg/m^3, Figure 5). Variations in PM_{10} concentrations for 2020 vs. 2019 were similar to those of $PM_{2.5}$ during Lock_1 and Soft (decreases up to –23%) and significantly lower during Lock_2, with increases of +9% (UT) and +28% (UB stations). Overall, during Lock_2, PM_{10} median concentrations increased by +1 to +2.8 μg/m^3, such that PM_{10} median values ranged between 19.3 and 23 μg/m^3 (Figure S7d).

4. Discussion

4.1. Air Quality Pattern during the Three Periods

4.1.1. Lock_1

During the most restrictive period in 2020 (Lock_1, Table S2), across all urban areas, road traffic reduced by −70 to −74%, proving to be strongly anticorrelated to SI (*r* ranging between −0.795 and −0.915). Except in Florence (−1%), gas consumption resulted in a slight increase (+7%) in Turin and Milan and in a significant increase (+20%) in Bologna (Table S7), thus reflecting the *T* pattern, which did not appreciably vary in Florence, while it slightly decreased elsewhere (−3 to −8%). Overall, in Italy in 2020, the meteorological conditions during Lock_1 were basically the same as in 2019 (Figures 2–5).

In this scenario, NO_2 concentrations experienced a drastic decrease, lower in Milan (up to −10.5 μg/m^3) and higher elsewhere (up to −24.7 μg/m^3 in Florence). These quotas are consistent with the median decrease in NO_2 concentrations (−19 μg/m^3) found

throughout Europe by [2]. The highest percent of NO_2 reductions (ranging between −41.9 and −53.9%) was lower than the reduction in total traffic (−70 to −74%). This is likely due to the increase in delivery and e-commerce, leading to a lower reduction in heavy-duty traffic than total traffic: compared to the corresponding months in 2019, at region-level heavy-duty traffic reduced by −7 to −27% in March 2020 and by −19 to −47% in April 2020, while total traffic reductions were equal to −53 to −63% and −72 to −79%, respectively [40,41]. In fact, heavy-duty vehicles—which are mostly diesel-fueled—emit a significant amount of overall road transport NO_x emissions (25.6% in Turin, 38.2% in Milan, 38.4% in Florence, and 38.5% in Bologna, Table S6). This outcome is confirmed by the moderate but not particularly high correlation of NO_2 concentrations with total traffic reduction (r = 0.584), a value similar to those (0.56 and 0.66) found during Lock_1 at two air quality stations in Padua (Italy) [42]. This correlation is also comparable to the overall value (R^2 = 0.343) found worldwide during the full lockdown periods [9]. By comparison, a higher (anti)correlation was observed between NO_2 concentrations and SI (r ranging between −0.649 and −0.832).

O_3 levels remained unchanged in Florence while slightly increasing elsewhere, particularly in Milan and Turin, where they rose by up to +17%, i.e., up to +5.1 and +8.8 μg/m^3, respectively. This O_3 pattern in Italy is again in line with the relative changes (−1 to +15%) reported throughout Europe by [2], and slightly higher than the continental-wide average (+5.6%) reported by [9]. Agreeing with various authors (e.g., [43]), these O_3 increases were mainly due to the reduction in nitrogen oxide (NO) emitted from road vehicles, leading to lower O_3 consumption via titration ($NO + O_3 = NO_2 + O_2$). Across European regions where the background level of NO_x is generally high, in April 2020, enhanced concentrations of oxidants including O_3 were observed. Consistently with [2], O_3 concentrations are significantly correlated with SI (r ranging between 0.576 and 0.762).

The drastic road traffic abatement during Lock_1 caused marginal effects on $PM_{2.5}$ and PM_{10}, as $PM_{2.5}$ varied at most between −2 and +3 μg/m^3, and PM_{10} between −2 and +4.5 μg/m^3. In percent terms, $PM_{2.5}$ varied between −21 and +18%, while PM_{10} varied between −23 and +9%, exhibiting lower decreases than the European median values (−10% for $PM_{2.5}$ and −23% for PM_{10} [2]). This outcome agrees with findings reported at the global scale by [9], who did not find any significant correlation during lockdowns between traffic flows and $PM_{2.5}$ concentrations. Since road transport contribution to emissions of both primary PM and secondary PM precursors (i.e., NO_x and NH_3) is generally remarkable (Table S4), both primary and secondary PM proved to be marginally affected by road traffic reduction during Lock_1. As observed locally (e.g., [16]) and elsewhere (e.g., [44]), this limited PM decrease likely results from an increase in gas consumption, and thus in domestic biomass burning during the "stay home" period, resulting in a slight increase in primary PM emissions. In Italy, biomass heating systems account for most of the overall primary $PM_{2.5}$ and PM_{10} emissions from heating plants (Table S5). Statistics from the PREPAIR project, updated to 2019 [45], report a mean percentage of biomass users in the Po Valley equal to 22%, with values of 14.4% in the Lombardy region (Milan), 18.5% in Emilia-Romagna (Bologna), and 26.2% in Piedmont (Turin). A further cause may be the increase in secondary PM, driven by an increase in emissions of precursors such as NH_3 on the one hand, and an increase in O_3 levels on the other. The Po Valley is one of the largest NH_3-emitting regions in Europe [46]: although no appreciable variation was recorded in 2020 with respect to the previous year [47], NH_3 emissions remained high enough in the region to support the formation of secondary aerosol [16]. On the other hand, as evidenced by various authors (e.g., [5,48]), increases in O_3 levels lead to an increased atmospheric oxidizing capacity, and thus an enhanced formation of secondary aerosol. Evidence of this outcome over the Po Valley has been provided by [46], who highlighted the increase in $PM_{2.5}$ levels due to enhanced non-linear photochemical processes triggered by NO_x emissions reduction.

4.1.2. Soft

Partial relaxation of restriction measures (Soft period) saw a generalized recovery of economic and social activities, and thus of road traffic, which, however, remained below the corresponding 2019 values (−11 to −24%). Road traffic reduction was less (anti)correlated with SI (*r* between −0.409 and −0.586) than during Lock_1. These traffic reduction quotas are quite similar to those (−17 to –27%) found in Madrid and Barcelona (Spain) between June and July 2020 [21], as well as to the value (−19%) found in London (UK) between May and July 2020, the one (−20%) found in Athens (Greece) between May and mid-June 2020, and the value (−16%) found in Paris (France) in June 2020 [9]. By contrast, during this period, traffic increases were observed in Germany (+22 to +29%), Moscow (Russia, +28%), and Helsinki (Finland, +31%) [9].

With heating systems turned off, during this period, road traffic played a major role among emission sources, resulting in a generalized decrease in NO_2 concentrations that ranged (except in Bologna, +7%) between −11 and −34%. However, an *r* value never exceeding 0.307 was found between NO_2 concentrations and road traffic. Observed NO_2 reductions agree with those (−10 to −31%) observed over main urban areas in Spain by [21] during the period June–July 2020, as well as with those found during the partial/full relaxation periods in various cities in Germany (−18 to −34%) and the Netherlands (−20 to −35%) by [9]. During Soft, the 2020 meteorological scenario was quite similar to 2019, with the notable exception of *H*, which increased up to +17%, thus favouring atmospheric pollutant dispersion.

With $PM_{2.5}$ and PM_{10} concentrations settled to their minimum values (at most 12 and 21.3 μg/m^3, respectively, Table S7), O_3 remained the most concerning pollutant for the season (*r* = 0.790 vs. *T*), particularly if considering the drop in NO road traffic emissions reducing O_3 titration [44]. Consistently with global-scale findings by [9], in Italy, O_3 median concentrations did not appreciably change during Soft vs. 2019, overall ranging between −10 and +7%, corresponding to variations of −8.1 and + 6.5 μg/m^3. If considering a climatologically similar country (Spain), 2020 vs. 2019 O_3 changes in Italy were similar to those (−3.5 to +7%) found in Valencia during the period June–September 2020 [6], as well as to those (−8.3 to +0.9%) observed in Madrid, Barcelona and Seville between mid-May and August 2020 [9].

4.1.3. Lock_2

In Italy, the second lockdown (Lock_2) was enforced in a period of the year that is typically critical for air quality, particularly over the Po Valley [22]. A significant reduction in road traffic occurred, with median values between −30 and −44% (Table S7) and the 5th-to-95th percentile range was between −10 and −71%. This, combined with a general increase in gas consumption (+2 to +14%), and thus of biomass burning for heating, was driven by appreciably lower *T* values (−1 to −1.5 °C). The whole 2020 meteorological scenario was also unfavourable with respect to 2019 for the other variables, as *WS* decreased by −12 to −28%, *H* by −3 to −31%, and *Prec* by −79 to −95%. These variables resulted in median decreases of up to −0.6 m/s for *WS*, −73 m for *H*, and −0.8 mm for *Prec*.

During this period, NO_2 concentrations were moderately correlated with road traffic (*r* = 0.321 − 0.503), experiencing—except at UT stations in Bologna (+22%) and at UB stations in Milan (−46.5%)—a moderate decrease in the median values (−11 to −26%, Table S7). O_3 concentrations confirmed to be at the lowest annual values, at most reaching 29.8 μg/m^3 in Florence. By contrast, a relevant increase in $PM_{2.5}$ and PM_{10} concentrations was observed, particularly in Turin and Milan. With median values of *WS* = 0.9 m/s, *T* = 5.9 °C, *H* = 110.7 m, and *Prec* = 0.3 mm, in Turin, for example, at UT stations, $PM_{2.5}$ median concentrations increased from 26 to 40 μg/m^3, while PM_{10} median concentrations increased from 33 to 54.8 μg/m^3. In Turin, during Lock_2, the days per station with PM_{10} concentrations exceeding the daily limit value (50 μg/m^3) was 2.7 times higher in 2020 than in 2019 (235 vs. 87). In Milan, with median values of *WS* = 1.2 m/s, *T* = 7.4 °C, *H* = 115.7 m, and

Prec = 0.2 mm, at UT stations, $PM_{2.5}$ median concentrations increased from 20 to 42 μg/m³, while PM_{10} median concentrations increased from 30.1 to 46.4 μg/m³. Here, during Lock_2, the days per station with PM_{10} concentrations exceeding the daily limit value was in 2020 2.4 times higher than in 2019 (169 vs. 69). Remarkably, in Turin and Milan (as well as in the rest of the Po Valley), the majority of these increases vs. 2019 occurred in Nov. rather than in Dec. 2020.

In the Po Valley, PM wintertime accumulation is mostly driven by local anthropogenic emissions due to: (i) heating plants, responsible for emissions of primary PM; (ii) road traffic, responsible for emissions of primary PM and secondary PM precursors (NH_3 and particularly NO_x); and (iii) agriculture activities, responsible for NH_3 emissions leading to the formation of secondary PM. During Lock_2, primary PM decrease due to road traffic reduction was counterbalanced by an increase likely resulting from higher biomass burning. During this period of the year, however, the secondary aerosol is predominant over the primary [46], proving to be a key factor controlling PM_{10} critical episodes in Northern Italy [27]. Secondary PM is generally dominated here by ammonium nitrate, whose fraction in winter may equal 4–5 times that of ammonium sulfate [46]. An analysis of PM_{10} chemical composition at the UB station of Pascal in Milan (Figure 1) by [49] accounted for the strong increase in monthly PM_{10} concentrations observed in Nov. 2020 vs. Nov. 2019. The drop in NO_x emissions due to road traffic reduction in Nov. 2020 did not suffice to decrease the potential of agriculture-related NH_3 emissions in the formation of ammonium nitrate: this outcome was also favoured by the less advective atmospheric conditions as well as by lower temperatures that favoured the partitioning of ammonium nitrate towards the particulate phase [46]. An increase in PM_{10} crustal fraction (primary component) was also observed, likely due to drier weather conditions that favoured dust resuspension. Unlike in the Po Valley, in Florence, the increase in PM concentrations vs. 2019 mainly occurred in Dec. 2020, likely because of the increase in PM primary fraction resulting from increased heating usage.

As an indirect confirmation of these findings, $PM_{2.5}$ and PM_{10} concentrations were not correlated with road traffic ($r = 0.086 - 0.245$), while they were moderately (anti)correlated with meteorological variables such as *Prec* ($r = -0.386$), *H* ($r = -0.507$), and *WS* ($r = -0.586$). These results reveal that unfavourable weather conditions for pollutant dispersion coupled with lockdown measures (that reduce road traffic but increase residential heating usage) lead to negative air quality conditions. A severe traffic ban extended all over the country and lasting more than two months was not enough to reduce $PM_{2.5}$ and PM_{10} levels, which increased due to unfavourable meteorological conditions.

4.2. Further Insight into the Lock_2 Period

In order to achieve a comprehensive picture of the scenario affecting the four urban areas during the Lock_2 period, the SOM algorithm was applied to a dataset including 12 variables. These are the daily time series of 2020 vs. 2019 absolute differences over all urban areas calculated for meteorological variables (*WS*, *T*, *H*, *R_dsw*, and *Prec*), anthropogenic emission drivers (*Gas* and *Flows*), and total pollutant concentrations (NO_2, O_3, $PM_{2.5}$, and PM_{10}); the 2020 SI was also included for comparison. The SOMs were calculated based on an input layer, including 272 neurons ($N_{samples}$) corresponding to the daily dataset of the 12 selected variables, and an output layer, including $N_{grid} = N_r x N_c = 64$ neurons, visualized by gridded hexagons with $N_r = 8$ rows and $N_c = 8$ columns. Following recommendations by [50], the map grid size ($N_{grid} = 64$) was taken as a value not higher than $5\sqrt{N_{samples}} = 82$ The result of the SOM application is presented in Figure 6.

The SOM algorithm proved capable of clustering all selected variables in the map retaining their mutual relationships, thus allowing to address a deeper cross-site investigation than that achieved by a simple linear analysis. During the Lock_2 period, the SOM component planes plotted in Figure 6 show that min-to-max orientation of NO_2 concentration variation (*dNO₂_tot*, hexagons oriented from top-right to bottom-left) is not exactly

the same as road traffic variation (*dFlows*), thus confirming their moderate but not particularly high mutual relationship. Comparing the SOMs of NO_2 and O_3 concentration variations (*dNO₂_tot* and *dO₃_tot*), O_3 increases (positive values) are associated to both NO_2 decreases (negative values) and NO_2 increases (positive values), while the opposite applies to O_3 decreases (negative values). Therefore, during Lock_2, the relation between O_3 and NO_2 concentrations is uncertain. Focusing on the SOMs of $PM_{2.5}$ and PM_{10} concentration variations (*dPM2.5_tot* and *dPM10_tot*), they can be clearly superimposed. Remarkably, the min-to-max topology of their neurons (i.e., from negative values corresponding to maximum decreases, to positive values corresponding to maximum increases) is similar to the max-to-min topology of variations in *WS*, *H*, and *Prec* (i.e., decreases of these variables). The same does not apply with respect to max-to-min topology of *dFlows* (i.e., from maximum to minimum road traffic decreases). As for *dGas*, the association is unclear, as increases in $PM_{2.5}$ and PM_{10} concentrations (left-hand side of *dPM2.5_tot* and *dPM10_tot*) are linked to both increases and decreases in gas consumption. Thus, the overall analysis reveals that increases in $PM_{2.5}$ and PM_{10} concentrations are strongly associated with decreases in *WS*, *H*, and *Prec*, marginally associated with traffic-related emission increases, and unclearly associated with biomass burning increases. A further outcome is that the SOM topology of $PM_{2.5}$ and PM_{10} variations is not particularly similar to SI variation: although minimum values of *dPM2.5_tot* and *dPM10_tot* (i.e., $PM_{2.5}$ and PM_{10} maximum decreases, maps' top-right hexagons) are associated with maximum values of SI (strongest restrictions), largely positive values and even maximum values of *dPM2.5_tot* and *dPM10_tot* (concentration increases, left-hand side) are associated with high values of SI. As a confirmation, $PM_{2.5}$ and PM_{10} variations are poorly anticorrelated with SI (r ranging between −0.009 and −0.226). This means that to enforce generalized strong limitations to anthropogenic activities—not only transportation—does not necessarily result in reducing $PM_{2.5}$ and PM_{10} values, whose critical levels—as discussed in Section 4.1.3—are both directly and indirectly controlled by the weather conditions.

The SOMs are confirmed as a powerful and insightful tool for analyzing the complex dynamics underlying the critical accumulation of PM in urban areas, being able to capture both the direct (linear) relations between primary PM emissions and concentrations, and the indirect (non-linear) interactions lying behind the formation of secondary PM. These findings concur with various studies worldwide (e.g., [51–55]). They provide a further confirmation of the crucial role played by meteorological conditions in driving the most critical $PM_{2.5}$ and PM_{10} concentrations, even when such drastic changes in specific human activities occur.

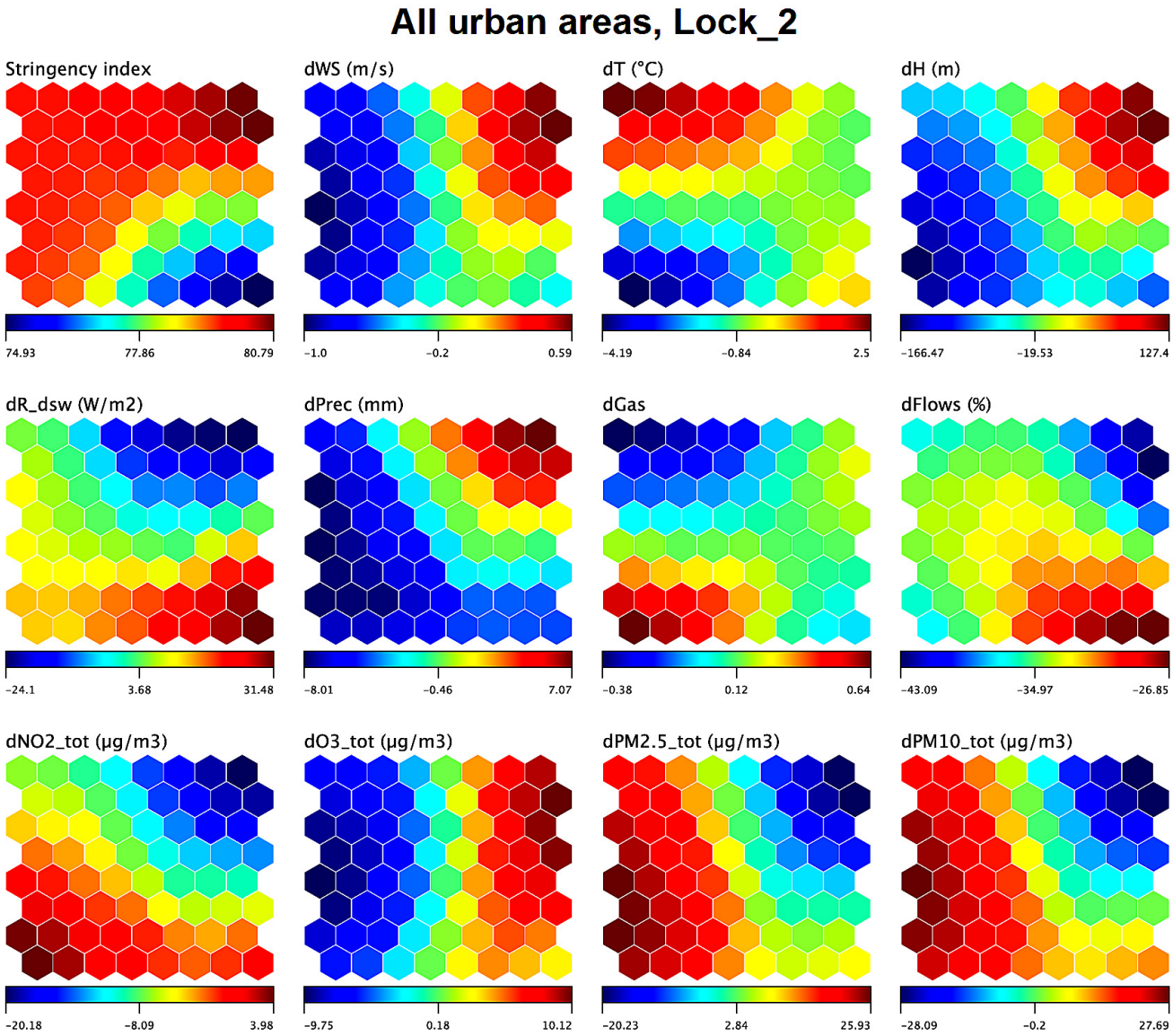

Figure 6. SOM component planes obtained in the urban areas of Turin, Milan, Bologna, and Florence during the Lock_2 period (23/10/2020–29/12/2020) from daily observations. The 12 panels report the 2020 Stringency index and the absolute difference of meteorological variables (*WS*, *T*, *H*, *R_dsw*, and *Prec*), anthropogenic emission drivers (*Gas* and *Flows*), and total pollutant concentrations (NO_2, O_3, $PM_{2.5}$, and PM_{10}) with respect to the 2019 baseline period (25/10/2019–31/12/2019). For 2020 vs. 2019 absolute differences, positive (negative) values mean increases (decreases). The panels are linked by position, so the hexagons in a certain position correspond to the same map unit.

5. Conclusions

During the first lockdown after the outbreak of the COVID-19 pandemic in early 2020, only NO_2 concentrations decreased systematically (and significantly, between −41.9 and −53.9%) in Italy with respect to the previous year, mainly because of the drastic road traffic reduction (−70 to −74%). O_3 levels slightly increased (up to +17%) due to the lower O_3 consumption due to the reduced NO emissions, while $PM_{2.5}$ and PM_{10} concentrations exhibited a contrasting behaviour: $PM_{2.5}$ varied between −21 and +18%, while PM_{10} varied between −23 and +9%. Primary PM decrease induced by road traffic reduction was counterbalanced by an increase due to higher heating usage (up to +20%). Concurrent secondary PM increased, likely because of relevant NH_3 emissions from agriculture [16] associated with an enhanced atmospheric oxidizing capacity [46].

During the summer period with partially relaxed measures, characterized by a moderate road traffic reduction (−11 to −24%), no particular air quality issue was observed, which was also the case with the O_3 levels, overall varying between −10 and +7% compared to the previous year.

The second (autumn/winter) lockdown in 2020 was particularly critical in terms of air quality, as the $PM_{2.5}$ and PM_{10} concentrations strongly increased (up to +87 and +123%, respectively) in spite of a significant road traffic reduction (−30 to −44%) lasting more than two months and involving the whole country. The PM primary component linked to traffic emissions clearly decreased. Particularly over the Po Valley, however, a traffic-related drop in NO_x emissions did not suffice to lower the potential of agriculture-related NH_3 emissions in the formation of ammonium nitrate, and thus in the increase in secondary PM.

This study revealed that, although non-linear interactions control the formation of secondary PM, which is generally the predominant fraction in winter [46], unfavourable meteorological conditions remain the main driver of PM most critical concentrations, even when such drastic changes in human activities occur. Findings from several studies in the literature (e.g., [42,53,55,56]) also confirmed that, markedly during this period of the year, road traffic restrictions alone are useless actions to prevent PM critical episodes in urban areas. For example, a study carried out by [46] in the Po Valley demonstrated poor (or even counterproductive) results when a proper combination of NO_x and NH_3 emission reductions was not implemented, confirming that PM reductions cannot be achieved without a significant reduction in NH_3 emissions from agriculture. The actions needed to achieve a generalized decarbonization and air quality improvement in modern societies must necessarily be cross-sectorial and not limited to transportation or other emission categories. Sector-specific actions do not necessarily result in pollutant concentration reductions, even when these restrictions apply through a prolonged time period (more than two months) and involve a whole country.

Supplementary Materials: The following supporting information can be downloaded at: https://www.mdpi.com/article/10.3390/atmos13071156/s1, Table S1: Characteristics of the four urban areas selected in the study; Table S2: Restriction periods in the year 2020 analysed in the study; Table S3: Characteristics of air quality stations by study area used in the study; Table S4: Share (%) by EU SNAP classification of overall yearly emissions of NO_x, NH_3, and primary $PM_{2.5}$ and PM_{10} in the municipality of Turin, Milan, Bologna and Florence based on the most updated regional emission inventories; Table S5: Share (%) by fuel type of yearly emissions of NO_x, NH_3, and primary $PM_{2.5}$ and PM_{10} from non-industrial combustion plants in the municipality of Turin, Milan, Bologna and Florence based on the most updated regional emission inventories; Table S6: Share (%) by vehicle category of yearly emissions of NO_x, NH_3, and primary $PM_{2.5}$ and PM_{10} from road transport in the municipality of Turin, Milan, Bologna and Florence based on the most updated regional emission inventories; Table S7: Median values and 2020 vs. 2019 median change rates by study area and period of meteorological parameters, anthropogenic emission drivers and pollutant concentrations; Figure S1: Daily pattern of the stringency index affecting Italy during the year 2020. The three restriction periods analysed, and corresponding stringency index average values are also shown; Figure S2: Scatterplot of daily gas consumption vs. mean air temperature observed in the city of Florence during the first six months of 2019 and 2020. Gas consumption is normalized to the whole municipality and to the 2019–2020 overall average. Temperature and gas consumption values are averaged over intervals of 0.5 °C. The best-fit linear equations and related R^2 values of the two data subsets are also shown; Figure S3: Daily time series by study area of pollutant emissions anthropogenic drivers during the 2020 restriction periods: (**a**) (estimated) gas consumption; (**b**) (observed) road traffic. Gas consumption estimations are normalized to the 2019–2020 overall average (1 meaning values aligned to this average), while road traffic observations are normalized to the 2019 overall average (0% meaning no variation vs. 2019). The average values by period of the stringency index are also shown; Figure S4: Boxplots of daily pollutant concentrations by period and station type observed in Turin: (**a**) NO_2; (**b**) O_3; (**c**) $PM_{2.5}$; (**d**) PM_{10}. Boxplots are delimited by the first (Q_1) and third (Q_3) distribution's quartiles, while the black line inside the box denotes the median value (Q_2). Lower whisker is $Q_1 - 1.5*IQR$, while upper whisker is $Q_3 + 1.5*IQR$, where the interquartile range (IQR) is $Q_3 - Q_1$. Circles outside the whiskers denote outlier data; Figure S5: Boxplots of daily pollutant concentrations by period and station type observed in Milan: (**a**) NO_2; (**b**) O_3; (**c**) $PM_{2.5}$; (**d**) PM_{10}.

Boxplots are delimited by the first (Q_1) and third (Q_3) distribution's quartiles, while the black line inside the box denotes the median value (Q_2). Lower whisker is $Q_1 - 1.5*IQR$, while upper whisker is $Q_3 + 1.5*IQR$, where the interquartile range (IQR) is $Q_3 - Q_1$. Circles outside the whiskers denote outlier data; Figure S6: Boxplots of daily pollutant concentrations by period and station type observed in Bologna: (**a**) NO_2; (**b**) O_3; (**c**) $PM_{2.5}$; (**d**) PM_{10}. Boxplots are delimited by the first (Q_1) and third (Q_3) distribution's quartiles, while the black line inside the box denotes the median value (Q_2). Lower whisker is $Q_1 - 1.5*IQR$, while upper whisker is $Q_3 + 1.5*IQR$, where the interquartile range (IQR) is $Q_3 - Q_1$. Circles outside the whiskers denote outlier data; Figure S7: Boxplots of daily pollutant concentrations by period and station type observed in Florence: (**a**) NO_2; (**b**) O_3; (**c**) $PM_{2.5}$; (**d**) PM_{10}. Boxplots are delimited by the first (Q_1) and third (Q_3) distribution's quartiles, while the black line inside the box denotes the median value (Q_2). Lower whisker is $Q_1 - 1.5*IQR$, while upper whisker is $Q_3 + 1.5*IQR$, where the interquartile range (IQR) is $Q_3 - Q_1$. Circles outside the whiskers denote outlier data.

Author Contributions: Conceptualization, G.G., and B.G.; methodology, G.G.; software, G.G.; investigation, G.G., and B.G.; validation, G.G.; data curation, G.G., L.B., F.C., and B.G.; visualization, G.G., and L.B.; writing—original draft preparation, G.G.; writing—review and editing, L.B., F.C., C.V., A.Z., and B.G.; supervision, B.G. All authors have read and agreed to the published version of the manuscript.

Funding: This research received no external funding.

Institutional Review Board Statement: Not applicable.

Informed Consent Statement: Not applicable.

Data Availability Statement: Not applicable.

Acknowledgments: The authors wish to thank "5T srl" for kindly providing the road mobility data of the city of Turin, and Vincenza Giancristiano (Tuscany Region) for kindly providing the emission data of the city of Florence.

Conflicts of Interest: The authors declare no conflicts of interest.

References

1. Sharifi, A.; Khavarian-Garmsir, A.R. The COVID-19 pandemic: Impacts on cities and major lessons for urban planning, design, and management. *Sci. Total Environ.* **2020**, *749*, 142391. https://doi.org/10.1016/j.scitotenv.2020.142391.
2. Gkatzelis, G.I.; Gilman, J.B.; Brown, S.S.; Eskes, H.; Gomes, A.R.; Lange, A.C.; McDonald, B.C.; Peischl, J.; Petzold, A.; Thompson, C.R.; et al. The global impacts of COVID-19 lockdowns on urban air pollution: A critical review and recommendations. *Elem. Sci. Anth.* **2021**, *9*, 00176. https://doi.org/10.1525/elementa.2021.00176.
3. Usman, M.; Ho, Y.S. COVID-19 and the emerging research trends in environmental studies: A bibliometric evaluation. *Environ. Sci. Pollut. Res.* **2021**, *28*, 16913–16924. https://doi.org/10.1007/s11356-021-13098-z.
4. Casado-Aranda, L.A.; Sánchez-Fernández, J.; Viedma-del-Jesús, M.I. Analysis of the scientific production of the effect of COVID-19 on the environment: A bibliometric study. *Environ. Res.* **2021**, *193*, 110416. https://doi.org/10.1016/j.envres.2020.110416.
5. Adam, M.G.; Tran, P.T.; Balasubramanian, R. Air quality changes in cities during the COVID-19 lockdown: A critical review. *Atmos. Res.* **2021**, *264*, 105823. https://doi.org/10.1016/j.atmosres.2021.105823.
6. Donzelli, G.; Cioni, L.; Cancellieri, M.; Llopis-Morales, A.; Morales-Suárez-Varela, M. Relations between Air Quality and Covid-19 Lockdown Measures in Valencia, Spain. *Int. J. Environ. Res. Public Health* **2021**, *18*, 2296. https://doi.org/10.3390/ijerph18052296.
7. Cucciniello, R.; Raia, L.; Vasca, E. Air quality evaluation during COVID-19 in Southern Italy: The case study of Avellino city. *Environ. Res.* **2022**, *203*, 111803. https://doi.org/10.1016/j.envres.2021.111803.
8. Pandey, M.; George, M.P.; Gupta, R.K.; Gusain, D.; Dwivedi, A. Impact of COVID-19 induced lockdown and unlock down phases on the ambient air quality of Delhi, capital city of India. *Urban Clim.* **2021**, *39*, 100945. https://doi.org/10.1016/j.uclim.2021.100945.
9. Sokhi, R.S.; Singh, V.; Querol, X.; Finardi, S.; Targino, A.C.; de Fatima Andrade, M.; Pavlovic, R.; Garland, R.M.; Massagué, J.; Kong, S.; et al. A global observational analysis to understand changes in air quality during exceptionally low anthropogenic emission conditions. *Environ. Int.* **2021**, *157*, 106818. https://doi.org/10.1016/j.envint.2021.106818.
10. Akritidis, D.; Zanis, P.; Georgoulias, A.K.; Papakosta, E.; Tzoumaka, P.; Kelessis, A. Implications of COVID-19 Restriction Measures in Urban Air Quality of Thessaloniki, Greece: A Machine Learning Approach. *Atmosphere* **2021**, *12*, 1500. https://doi.org/10.3390/atmos12111500.
11. Chen, L.W.A.; Chien, L.C.; Li, Y.; Lin, G. Nonuniform impacts of COVID-19 lockdown on air quality over the United States. *Sci. Total. Environ.* **2020**, *745*, 141105. https://doi.org/10.1016/j.scitotenv.2020.141105.

12. Dantas, G.; Siciliano, B.; Franca, B.B.; da Silva, C.M.; Arbilla, G. The impact of COVID-19 partial lockdown on the air quality of the city of Rio de Janeiro, Brazil. *Sci. Total Environ.* **2020**, *729*, 139085. https://doi.org/10.1016/j.scitotenv.2020.139085.
13. Shakoor, A.; Chen, X.; Farooq, T.H.; Shahzad, U.; Ashraf, F.; Rehman, A.; Sahar, N.E.; Yan, W. Fluctuations in environmental pollutants and air quality during the lockdown in the USA and China: Two sides of COVID-19 pandemic. *Air Qual. Atmos. Health* **2020**, *13*, 1335–1342. https://doi.org/10.1007/s11869-020-00888-6.
14. Gualtieri, G.; Brilli, L.; Carotenuto, F.; Vagnoli, C.; Zaldei, A.; Gioli, B. Quantifying road traffic impact on air quality in urban areas: A Covid19-induced lockdown analysis in Italy. *Environ. Pollut.* **2020**, *267*, 115682. https://doi.org/10.1016/j.envpol.2020.115682.
15. Pei, Z.; Han, G.; Ma, X.; Su, H.; Gong, W. Response of major air pollutants to COVID-19 lockdowns in China. *Sci. Total Environ.* **2020**, *743*, 140879. https://doi.org/10.1016/j.scitotenv.2020.140879.
16. Putaud, J.P.; Pozzoli, L.; Pisoni, E.; Dos Santos, S.M.; Lagler, F.; Lanzani, G.; Dal Santo, U.; Colette, A. Impacts of the COVID-19 lockdown on air pollution at regional and urban background sites in northern Italy. *Atmos. Chem. Phys.* **2021**, *21*, 7597–7609. https://doi.org/10.5194/acp-21-7597-2021.
17. Wade, A.; Petherick, A.; Kira, B.; Tatlow, H.; Elms, J.; Green, K.; Hallas, L.; di Folco, M.; Hale, T.; Phillips, T.; et al. Variation in Government Responses to COVID-19. BSG-WP-2020/032, Version 13.0. March 2022. Available online: https://www.bsg.ox.ac.uk/research/publications/variation-government-responses-covid-19 (accessed on 7 June 2022).
18. Kumar, S.; Managi, S. Does stringency of lockdown affect air quality? Evidence from Indian cities. *Econ. Disasters Clim. Change* **2020**, *4*, 481–502. https://doi.org/10.1007/s41885-020-00072-1.
19. Dang, H.A.H.; Trinh, T.A. Does the COVID-19 lockdown improve global air quality? New cross-national evidence on its unintended consequences. *J. Environ. Econ. Manag.* **2021**, *105*, 102401. https://doi.org/10.1016/j.jeem.2020.102401.
20. Hersbach, H.; Bell, B.; Berrisford, P.; Hirahara, S.; Horányi, A.; Muñoz-Sabater, J.; Nicolas, J.; Peubey, C.; Radu, R.; Schepers, D.; et al. The ERA5 global reanalysis. *Q. J. R. Meteorol. Soc.* **2020**, *146*, 1999–2049. https://doi.org/10.1002/qj.3803.
21. Querol, X.; Massagué, J.; Alastuey, A.; Moreno, T.; Gangoiti, G.; Mantilla, E.; Duéguez, J.J.; Escudero, M.; Monfort, E.; García-Pando, C.P.; et al. Lessons from the COVID-19 air pollution decrease in Spain: Now what? *Sci. Total Environ.* **2021**, *779*, 146380. https://doi.org/10.1016/j.scitotenv.2021.146380.
22. Campanelli, M.; Iannarelli, A.M.; Mevi, G.; Casadio, S.; Diémoz, H.; Finardi, S.; Dinoi, A.; Castelli, E.; di Sarra, A.; Di Bernardino, A.; et al. A wide-ranging investigation of the COVID-19 lockdown effects on the atmospheric composition in various Italian urban sites (AER–LOCUS). *Urban Clim.* **2021**, *39*, 100954. https://doi.org/10.1016/j.uclim.2021.100954.
23. Hale, T.; Angrist, N.; Goldszmidt, R.; Kira, B.; Petherick, A.; Phillips, T.; Webster, S.; Cameron-Blake, E.; Hallas, L.; Majumdar, S.; et al. A Global Panel Database of Pandemic Policies (Oxford COVID-19 Government Response Tracker). *Nat. Hum. Behav.* **2021**, *5*, 529–538. https://doi.org/10.1038/s41562-021-01079-8.
24. Blavatnik School of Government, University of Oxford. Oxford COVID-19 Government Response Tracker. Available online: https://github.com/OxCGRT/covid-policy-tracker/blob/master/data/timeseries/stringency_index.csv (accessed on 7 June 2022).
25. ECMWF Reanalysis v5 (ERA5). Available online: https://www.ecmwf.int/en/forecasts/dataset/ecmwf-reanalysis-v5 (accessed on 7 June 2022).
26. ISPRA. Comparison between Energy Consumption and Heating Degree Days (HDD). Projections to 2050 of HDD in different climate scenarios. Report 277/2017. December 2017. Available online: https://www.isprambiente.gov.it/en/publications/reports/comparison-between-energy-consumption-and-heating-degree-days-hdd-.-projections-to-2050-of-hdd-in-different-climate-scenarios (accessed on 7 June 2022).
27. Gualtieri, G.; Carotenuto, F.; Finardi, S.; Tartaglia, M.; Toscano, P.; Gioli, B. Forecasting PM_{10} hourly concentrations in northern Italy: Insights on models performance and PM_{10} drivers through self-organizing maps. *Atmos. Pollut. Res.* **2018**, *9*, 1204–1213. https://doi.org/10.1016/j.apr.2018.05.006.
28. 5T srl. Traffic Flow Open Data. Available online: http://aperto.comune.torino.it/dataset/flussi-di-traffico (accessed on 7 June 2022). (In Italian)
29. Municipality of Milan. Open data. Available online: http://dati.comune.milano.it (accessed on 7 June 2022). (In Italian)
30. Municipality of Bologna. Mobility Open Data. Available online: https://opendata.comune.bologna.it/explore/dataset/bologna-daily-mobility/information (accessed on 7 June 2022). (In Italian)
31. Snap4City. Traffic Flow Data in Florence. Available online: https://www.snap4city.org/dashboardSmartCity/view/index.php?iddasboard=MTE5MQ (accessed on 7 June 2022).
32. ARPA Piedmont. IREA Regional Emission Inventory—2015 Emissions in the Piedmont Region. Available online: http://www.sistemapiemonte.it/fedwinemar/elenco.jsp (accessed on 7 June 2022). (In Italian)
33. ARPA Lombardy. INEMAR Regional Emission Inventory—2017 Emissions in the Lombardy Region. Available online: https://www.inemar.eu/xwiki/bin/view/InemarDatiWeb/Aggiornamenti+dell%27inventario+2017 (accessed on 7 June 2022). (In Italian)
34. ARPA Emilia-Romagna. INEMAR Regional Emission Inventory—2017 Emissions in the Emilia-Romagna Region. Available online: https://datacatalog.regione.emilia-romagna.it/catalogCTA/dataset/inventario-regionale-emissioni-in-atmosfera-inemar/resource/2e223430-b917-4e8f-a6ea-27f2a44cfac5 (accessed on 7 June 2022). (In Italian)
35. Tuscany Region. IRSE Regional Emission Inventory. Available online: https://www.regione.toscana.it/-/inventario-regionale-sulle-sorgenti-di-emissione-in-aria-ambiente-irse (accessed on 7 June 2022). (In Italian)

36. ISPRA. Ammonia Emissions from the Agricultural Sector. Available online: https://annuario.isprambiente.it/pon/basic/44 (accessed on 7 June 2022). (In Italian)
37. R Core Team. The R Project for Statistical Computing. Available online: https://www.r-project.org (accessed on 7 June 2022).
38. R Graphics Package. Available online: https://stat.ethz.ch/R-manual/R-devel/library/graphics/html/00Index.html (accessed on 7 June 2022).
39. Kohonen, T. *Self-Organizing Maps*, 2nd ed.; Springer: Heidelberg, Germany, 2001.
40. ANAS. Osservatorio del Traffico—Dati di Riferimento Marzo 2020. April 2020. Available online: https://www.stradeanas.it/sites/default/files/SMI4%20-%20Osservatorio%20del%20Traffico%20Marzo%202020.pdf (accessed on 7 June 2022). (In Italian)
41. ANAS. Osservatorio del Traffico—Dati di Riferimento Aprile 2020. May 2020. Available online: https://www.stradeanas.it/sites/default/files/SMI4%20-%20Osservatorio%20del%20Traffico%20Aprile%202020.pdf (accessed on 7 June 2022). (In Italian)
42. Rossi, R.; Ceccato, R.; Gastaldi, M. Effect of road traffic on air pollution. Experimental evidence from COVID-19 lockdown. *Sustainability* **2020**, *12*, 8984. https://doi.org/10.3390/su12218984.
43. Gaubert, B.; Bouarar, I.; Doumbia, T.; Liu, Y.; Stavrakou, T.; Deroubaix, A.; Darras, S.; Elguindi, N.; Granier, G.; Lacey, F.; et al. Global changes in secondary atmospheric pollutants during the 2020 COVID-19 pandemic. *J. Geophys. Res. Atmospheres* **2021**, *126*, e2020JD034213. https://doi.org/10.1029/2020JD034213.
44. Petit, J.E.; Dupont, J.C.; Favez, O.; Gros, V.; Zhang, Y.; Sciare, J.; Simon, L.; Truong, F.; Bonnaire, N.; Amodeo, T.; et al. Response of atmospheric composition to COVID-19 lockdown measures during spring in the Paris region (France). *Atmos. Chem. Phys.* **2021**, *21*, 17167–17183. https://doi.org/10.5194/acp-21-17167-2021.
45. Patti, S.; Pillon, S.; Intini, B.; Susanetti, L.; Francescato, V.; Rossi, D. Survey to Estimate Woody Biomasses Consumption in Households. Action D3. Residential Wood Consumption Estimation in the Po Valley. Project PREPAIR (LIFE 15 IPE IT 013). 1 February 2020. Available online: http://www.lifeprepair.eu/?smd_process_download=1&download_id=8196 (accessed on 7 June 2022).
46. Thunis, P.; Clappier, A.; Beekmann, M.; Putaud, J.P.; Cuvelier, C.; Madrazo, J.; de Meij, A. Non-linear response of $PM_{2.5}$ to changes in NO_x and NH_3 emissions in the Po basin (Italy): Consequences for air quality plans. *Atmos. Chem. Phys.* **2021**, *21*, 9309–9327. https://doi.org/10.5194/acp-21-9309-2021.
47. ARPA Lombardy. Valutazione Emissiva e Modellistica di Impatto sulla Qualità dell'Aria durante l'Emergenza COVID-19: Periodo Febbraio–Maggio. October 2020. Available online: https://www.arpalombardia.it/sites/DocumentCenter/Documents/Aria%20-%20Relazioni%20approfondimento/Emis-mod-report-stima-emissiva-COVID-19-lombardia_maggio20.pdf (accessed on 7 June 2022). (In Italian)
48. Huang, X.; Ding, A.; Gao, J.; Zheng, B.; Zhou, D.; Qi, X.; Tang, R.; Wang, J.; Ren, C.; Nie, W.; et al. Enhanced secondary pollution offset reduction of primary emissions during COVID-19 lockdown in China. *Natl. Sci. Rev.* **2021**, *8*, nwaa137. https://doi.org/10.1093/nsr/nwaa137.
49. ARPA Lombardy. Gli Effetti dei Provvedimenti di Limitazione delle Attività sulle Concentrazioni di $PM_{2.5}$ e sulla Composizione del PM_{10}. Available online: https://www.arpalombardia.it/sites/DocumentCenter/Documents/Aria%20-%20Relazioni%20approfondimento/$PM_{2.5}$-COVID_210318.pdf (accessed on 7 June 2022). (In Italian)
50. Vesanto, J.; Alhoniemi, E. Clustering of the self-organizing map. *IEEE Trans. Neural Netw.* **2000**, *11*, 586–600. https://doi.org/10.1109/72.846731.
51. Holst, J.; Mayer, H.; Holst, T. Effect of meteorological exchange conditions on PM_{10} concentration. *Meteorol. Z.* **2008**, *17*, 273–282. https://doi.org/10.1127/0941-2948/2008/0283.
52. Barmpadimos, I.; Hueglin, C.; Keller, J.; Henne, S.; Prévôt, A.S.H. Influence of meteorology on PM_{10} trends and variability in Switzerland from 1991 to 2008. *Atmos. Chem. Phys.* **2011**, *11*, 1813–1835. https://doi.org/10.5194/acp-11-1813-2011.
53. Invernizzi, G.; Ruprecht, A.; Mazza, R.; De Marco, C.; Močnik, G.; Sioutas, C.; Westerdahl, D. Measurement of black carbon concentration as an indicator of air quality benefits of traffic restriction policies within the ecopass zone in Milan, Italy. *Atmos. Environ.* **2011**, *45*, 3522–3527. https://doi.org/10.1016/j.atmosenv.2011.04.008.
54. Cai, H.; Xie, S. Traffic-related air pollution modeling during the 2008 Beijing Olympic Games: The effects of an odd-even day traffic restriction scheme. *Sci. Total Environ.* **2011**, *409*, 1935–1948. https://doi.org/10.1016/j.scitotenv.2011.01.025.
55. Gualtieri, G.; Toscano, P.; Crisci, A.; Di Lonardo, S.; Tartaglia, M.; Vagnoli, C.; Zaldei, A.; Gioli, B. Influence of road traffic, residential heating and meteorological conditions on PM_{10} concentrations during air pollution critical episodes. *Environ. Sci. Pollut. Res.* **2015**, *22*, 19027–19038. https://doi.org/10.1007/s11356-015-5099-x.
56. Duque, L.; Relvas, H.; Silveira, C.; Ferreira, J.; Monteiro, A.; Gama, C.; Rafael, S.; Freitas, S.; Borrego, C.; Miranda, A. Evaluating strategies to reduce urban air pollution. *Atmos. Environ.* **2016**, *127*, 196–204. https://doi.org/10.1016/j.atmosenv.2015.12.043.